JOURNAL PRE-PROOF

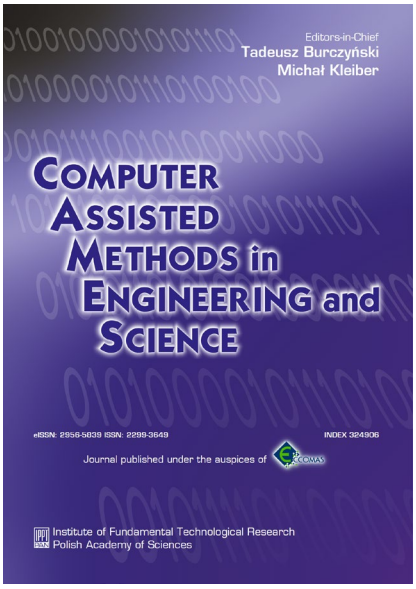

Title: Isogeometric Topology Optimization Based on Topological Derivatives

Author(s): Guilherme Henrique Teixeira, Nepomuk Krenn, Peter Gangl, Benjamin Marussig

DOI: https://doi.org/10.24423/cames.2026.1874

Journal: *Computer Assisted Methods in Engineering and Science*

ISSN: 2299-3649, e-ISSN: 2956-5839

Publication status: In press

Received: 2025-06-25

Revised: 2026-01-12

Accepted: 2026-01-17

Published pre-proof: 2026-01-20

Please cite this article as:

Teixeira G.H., Krenn N., Gangl P., Marussig B., Isogeometric Topology Optimization Based on Topological Derivatives, *Computer Assisted Methods in Engineering and Science*, 2026, https://doi.org/10.24423/cames.2026.1874

Isogeometric Topology Optimization Based on Topological Derivatives

Guilherme Henrique TEIXEIRA[1,*], Nepomuk KRENN[2], Peter GANGL[2], and Benjamin MARUSSIG[1]

[1]*Graz University of Technology, Institute of Applied Mechanics, Technikerstraße 4/II, 8010 Graz, Austria*

[2]*Johann Radon Institute for Computational and Applied Mathematics, Altenberger Straße 69, A-4040 Linz, Austria*

[*]*Corresponding Author e-mail: teixeira@tugraz.at*

Abstract

Topology optimization is a valuable tool in engineering, facilitating the design of optimized structures. However, topological changes often require a remeshing step, which can become challenging. In this work, we propose an isogeometric approach to topology optimization driven by topological derivatives. The combination of a level-set method together with an immersed isogeometric framework allows seamless geometry updates without the necessity of remeshing. At the same time, topological derivatives provide topological modifications without the need to define initial holes [7]. We investigate the influence of higher-degree basis functions in both the level-set representation and the approximation of the solution. Two numerical examples demonstrate the proposed approach, showing that employing higher-degree basis functions for approximating the solution improves accuracy, while linear basis functions remain sufficient for the level-set function representation.

Keywords: topology optimization, isogeometric analysis, topological derivative, level-set method, immersed methods, higher-degree basis function.

1 Introduction

Design optimization describes an iterative process to define the optimal geometry of a structure given some constraints. This problem can be approached in several ways, including the optimization of geometric parameters, such as radius, length, or width (Figure 1a), the boundaries of the shape (Figure 1b) [46], or the material distribution of the structure (Figure 1c) [26]. The last one is known as topology optimization,

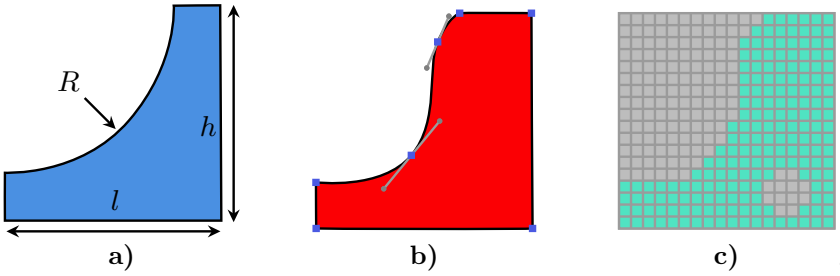

Figure 1: Different types of optimization: a) Parameter Optimization; b) Shape Optimization; c) Topology Optimization

and since it was first introduced in [9], several methods have been developed to approach the problem, and in consequence, various challenges have been addressed [36]. The most popular classes of topology optimization methods are based on design representations by means of density or level set functions.

Density-based approaches, widely used in topology optimization [36], represent the design through a density variable equal to 1 as material and 0 as void. These methods can be used in a fixed background mesh on which the density variable is defined element-wise, identifying if the element is solid or void, avoiding the need for remeshing during the optimization process. However, a well-known challenge of density-based topology optimization is the presence of unphysical intermediate materials, which is overcome through penalization techniques, such as the Solid Isotropic Material with Penalization (SIMP), removing gray areas and resulting in nearly black-and-white designs [13].

In level-set based approaches [29], the material distribution is represented by the sign of a continuous level-set function which is evolving in the course of the optimization process. Level set methods have been extensively applied to shape and topology optimization, either coupled with a remeshing strategy [15] or on a fixed background mesh [2, 3, 44]. The evolution of the level set function is either guided by shape derivatives via a Hamilton-Jacobi transport equation [2] or by topological derivatives [7]. In the former case, the resulting design heavily depends on the initial topology. New holes cannot be directly introduced, and it depends on the holes of the initial geometry, which can then be merged or cancelled in the optimization process. In order to allow for nucleation of new holes, the method has been coupled with topological derivatives in [1, 10]. Another possible approach combining the level-set method and topological derivatives without solving the Hamilton-Jacobi is proposed in [7], with many applications in the literature [27, 8, 25, 47, 11, 28, 16] and also extended to multi-material in [17]. In this algorithm, the optimization is guided only by the topological derivative.

Isogeometric analysis (IGA), first introduced in [21], presents the concept of connecting design and analysis using the same B-splines representing the geometry as basis functions. The straightforward control over the degree and smoothness of a B-spline basis is quite valuable for numerical simulations. Several

research studies have been done using the isogeometric concept in variations of topology optimization approaches. On the one hand, applications of the density method in the context of IGA have been reported in several studies in the literature [20], where a connection between the optimization and the CAD environments [34], and the benefits of refinement schemes straightforwardly connect with the approach [42, 38] are observed. On the other hand, the conventional level-set method was used with different discretizations for the level-set function, such as using radial basis functions [35, 4], B-splines [22], or piece-wise constant functions [23]. To the best of our knowledge, the combination of IGA and topological derivative-based level set optimization has only been considered in [30], where the conventional shape derivative-based level-set method extended by a topological derivative term was used.

In this work, we apply the approach of [7] within the isogeometric framework, using B-splines for both the level-set function discretization and as basis functions to approximate the solution. Compared to standard level-set methods, this approach has the following advantages: Since it uses a fixed background mesh, it eliminates the need for remeshing, and, by using the topological derivative to guide the evolution of the level-set function, it also removes the necessity of defining initial holes and does not require solving the Hamilton-Jacobi equation, relying only on the topological derivative to guide the evolution of the level-set function. In addition, compared to standard density-based methods, this approach does not introduce artificial intermediate materials, since it uses a level-set function to describe the design.

Our contribution focuses on the combination of the level-set method, topological derivatives, and isogeometric analysis, providing initial configurations free from geometric approximation errors and a simplified fixed high-degree background mesh defined by the knot vector and control points, which also allows straightforward higher-degree simulations. A challenge of this approach is the handling of the material interface, since we use a fixed mesh that does not adapt to the level-set function. We study the sensitivity of the level-set representation in the optimized topology due to different polynomial degrees for approximating the level-set function and the solution. To accomplish this, we investigate two different settings: One with the same polynomial degree for both, and the other one with a linear level-set function discretization and a higher-degree approximation of the solution.

Therefore, in Section 2, we present the linear elasticity problem investigated in the topology optimization approach and the main considerations for applying isogeometric analysis to it. Then, the definition of the level-set function and the derived topological derivative are provided, respectively, in Sections 3 and 4. In addition, Section 5 approaches the procedures to deal with the cut elements, and two numerical results applied to linear elasticity problems are shown in Section 6. Finally, in the conclusion, we summarize the main findings from the numerical examples.

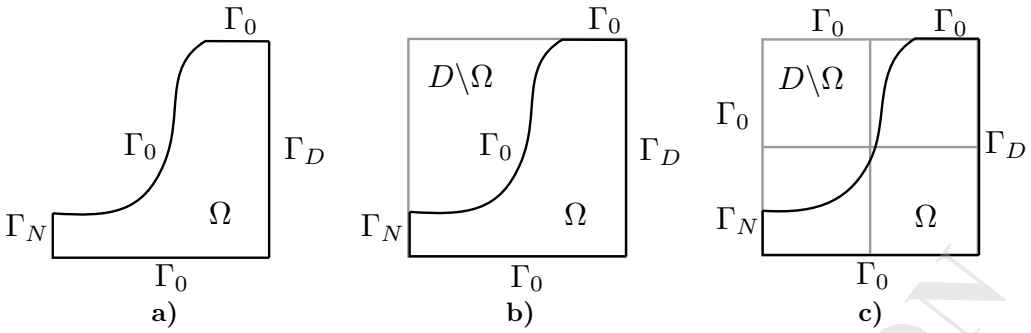

Figure 2: Representation of the domain problem: a) Domain Ω defined by the level-set; b) Domain Ω as a subset of domain D; c) Domain Ω inside of a B-spline background mesh defined from the knot vector of the geometry D

2 Problem Description

In this section, we present an overview of the problem to which our approach is applied. The problem studied is the compliance minimization in two-dimensional linear elasticity, and here we present the governing equation, the formulation of the minimization problem, and the key considerations for applying isogeometric analysis using an immersed approach based on the level-set method.

2.1 Linear Elasticity Problem

In this work, we consider linear elasticity problems defined on a domain Ω, where the boundary $\partial\Omega$ is divided into three disjoint parts, such that $\Gamma_D \cap \Gamma_N = \emptyset$, $\Gamma_D \cap \Gamma_0 = \emptyset$, $\Gamma_N \cap \Gamma_0 = \emptyset$ and $\Gamma_D \cap \Gamma_N \cap \Gamma_0 = \emptyset$, as shown in Figure 2a. In these three parts of the boundary, Dirichlet boundary conditions are applied in Γ_D, Neumann boundary conditions in Γ_N, and zero Neumann boundary conditions are applied in Γ_0. Therefore, the governing equations for the problem are given by

$$\begin{cases} -\nabla \cdot (\boldsymbol{\sigma}(\mathbf{u})) = \mathbf{0} & \text{in } \Omega \\ \mathbf{u} = \mathbf{0} & \text{on } \Gamma_D \\ \boldsymbol{\sigma}(\mathbf{u}) \cdot \mathbf{n} = \boldsymbol{\tau} & \text{on } \Gamma_N \\ \boldsymbol{\sigma}(\mathbf{u}) \cdot \mathbf{n} = \mathbf{0} & \text{on } \Gamma_0. \end{cases} \tag{1}$$

Here, $\boldsymbol{\tau}$ is the load applied on the boundaries and $\mathbf{n}$ is the normal vector on it. While $\mathbf{u}$ represents the displacement field and $\boldsymbol{\sigma}$ is the stress tensor, which for linear elasticity and isotropic materials is defined as

$$\boldsymbol{\sigma}(\mathbf{u}) = 2\mu\boldsymbol{\epsilon}(\mathbf{u}) + \lambda \operatorname{tr}(\boldsymbol{\epsilon}(\mathbf{u}))\mathbf{I},$$

where

$$\boldsymbol{\epsilon}(\mathbf{u}) = \frac{1}{2}\left(\nabla\mathbf{u} + (\nabla\mathbf{u})^T\right)$$

is the strain tensor and, for 2d plane strain,

$$\mu = \frac{E}{2(1+\nu)}, \quad \lambda = \frac{E\nu}{(1+\nu)(1-2\nu)}$$

are the Lamé parameters, written with respect to the Young modulus E and Poisson ratio ν.

In this scenario, the domain Ω represents the material distribution of the geometry and is a subset of a larger domain D. This situation is graphically represented by Figure 2b.

2.2 Immersed Isogeometric Approach

The goal of the topology optimization is to find an optimal material distribution Ω under given constraints, such as boundary conditions or area penalization. This can be formulated as a minimization problem. In this scenario, the domain Ω changes during the optimization process, and solving the problem numerically would require redefining the mesh at each iteration. To avoid the necessity of remeshing, we formulate the problem in the fixed domain D, as shown in Figure 2b, instead of Ω, shown in Figure 2a, and we introduce a material property alpha, which is equal to α_{in} if it is inside of Ω and a small value α_{out} for outside. This approach is based on immersed methods, which are extensively applied to fluid mechanics, solid mechanics, interface problems, and several other areas. An extensive explanation of immersed methods and their aspects can be found in [45, 12, 41]. In this way, this approach allows us to define which part of D represents Ω, in such a way that the governing equation for the linear elasticity problem can be rewritten as

$$\begin{cases} -\nabla\cdot(\alpha_\Omega\boldsymbol{\sigma}(\mathbf{u})) = \mathbf{0} & \text{in } D, \\ \mathbf{u} = \mathbf{0} & \text{on } \Gamma_D, \\ \boldsymbol{\sigma}(\mathbf{u})\cdot\mathbf{n} = \boldsymbol{\tau} & \text{on } \Gamma_N, \\ \boldsymbol{\sigma}(\mathbf{u})\cdot\mathbf{n} = \mathbf{0} & \text{on } \Gamma_0, \end{cases} \quad \text{with} \quad \alpha_\Omega = \begin{cases} \alpha_{in} & \text{in } \Omega, \\ \alpha_{out} & \text{on } D\setminus\overline{\Omega}, \end{cases} \tag{2}$$

where $\alpha_{out} \ll 1$ is a penalization parameter on the void, small enough to neglect the basis located outside the domain Ω, but not too small to result in an ill-conditioned stiffness matrix [33].

Therefore, to finally solve the problem numerically, we discretize the domain D using a background mesh, as shown in Figure 2c, where the basis functions used to approximate the solution field are B-splines of degree p, refined from the geometry D. These basis functions are constructed from a non-decreasing set

of coordinates called knot vector

$$\Xi = \{\xi_1, \xi_2, ..., \xi_{n+p}, \xi_{n+p+1}\} \tag{3}$$

defined in a parameter space $\mathbb{P} = [\xi_1, \xi_{n+p+1}]$ of B-splines, where n is the number of basis functions and p is the polynomial degree. This construction is defined recursively starting from piece-wise constant functions for $p = 0$

$$B_{i,0} = \begin{cases} 1 & \text{if } \xi_i \leq \xi < \xi_{i+1} \\ 0 & \text{otherwise} \end{cases}, \tag{4}$$

and extended for higher degrees $p > 0$ by applying the Cox-de Boor formula [21]

$$B_{i,p} = \frac{\xi - \xi_i}{\xi_{i+p} - \xi_i} B_{i,p-1}(\xi) + \frac{\xi_{i+p+1} - \xi}{\xi_{i+p+1} - \xi_{i+1}} B_{i+1,p-1}(\xi). \tag{5}$$

In sequence, having the basis functions in each parametric direction, the geometry mapping from the parametric domain $\mathbb{P}^2 = [\xi_1, \xi_{n+p+1}] \times [\eta_1, \eta_{m+p+1}]$ to the physical domains $\mathbb{R}^2$ is then defined as

$$\mathbf{x}(\xi, \eta) = \sum_{i=1}^{n} \sum_{j=1}^{m} B_{i,p}(\xi) B_{j,p}(\eta) \mathbf{C}_{i,j}, \tag{6}$$

where $\mathbf{C}_{i,j}$ are the control points that build the geometry.

Note that the basis functions used to approximate the solution field may have a different polynomial degree p than those used to construct the geometry D. However, the geometric mapping remains based on the B-splines defined from the geometry D. Finally, the implementation of the problem is made within an open-source isogeometric analysis code [43], which provides the necessary features.

2.3 Minimization Problem

The minimization problem mentioned in the previous subsection, and which defines the topology optimization process, has the goal of searching for the optimal domain $\Omega \subset D$ that minimizes a cost function J. This expression can be written as

$$\min_{\Omega \in \mathcal{E}} J(\Omega, \mathbf{u}), \tag{7}$$

where $\mathcal{E}$ is a set of admissible subsets of D and

$$J(\Omega, \mathbf{u}) = \int_D \alpha_\Omega \boldsymbol{\sigma}(\mathbf{u}) : \boldsymbol{\epsilon}(\mathbf{u}) \, dD + l \int_\Omega d\Omega. \tag{8}$$

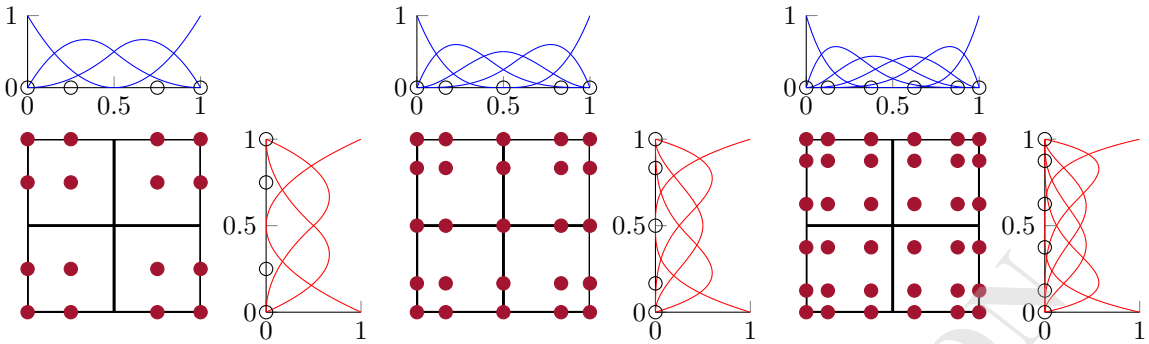

Figure 3: Distribution of the Greville abscissae on the elements for different polynomial degrees and basis functions defined by a) $\Xi = \{0\,0\,0\,0.5\,1\,1\,1\}$. b) $\Xi = \{0\,0\,0\,0\,0.5\,1\,1\,1\,1\}$. c) $\Xi = \{0\,0\,0\,0\,0\,0.5\,1\,1\,1\,1\,1\}$

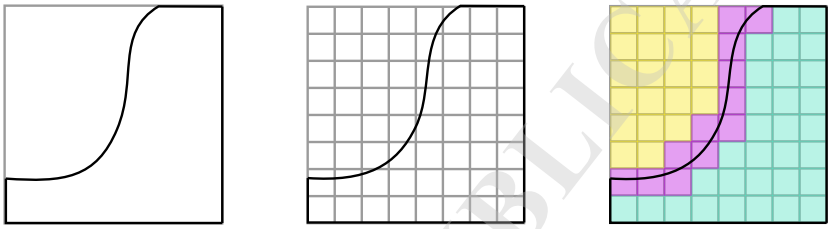

Figure 4: Type identification of the elements for assembling of the material property α: a) Domain D divided into two regions by a level-set function. b) Domains D discretized as the background mesh. c) Identification of the elements. In yellow, the elements are located outside of Ω. In blue, inside of Ω and in pink, the cut elements

Note that the area constraint, to avoid the solution to be $\Omega = D$, is addressed by the second term of the objective function and controlled by the parameter l [24].

3 Discretized Level-set Representation

The domain Ω is represented by a continuous level-set function. This means that the interface that divides the material region Ω from the void region $D \setminus \Omega$ is defined by the zero set of the level-set function. Specifically, all points where the level-set function is smaller than 0 belong to Ω, points where it is higher than zero belong to the void $D \setminus \Omega$, and points where the level-set function is equal to zero lie on the interface between the two regions

$$\begin{cases} \phi(\mathbf{x}) < 0 & \iff \mathbf{x} \in \Omega, \\ \phi(\mathbf{x}) = 0 & \iff \mathbf{x} \in \partial\Omega, \\ \phi(\mathbf{x}) > 0 & \iff \mathbf{x} \in D \setminus \overline{\Omega}. \end{cases} \tag{9}$$

As the background mesh D is discretized, we also discretize the domain Ω. Therefore, the level-set

discretization is made using B-spline basis functions of degree d, which might be the same or different from the degree p of the basis functions used for approximating the solution,

$$\phi(\xi,\eta)=\sum_{i=1}^{n}\sum_{j=1}^{m}B_{i,d}(\xi)B_{j,d}(\eta)c_{i,j}. \tag{10}$$

In sequence, the coefficients $c_{i,j}$ are obtained by solving a collocation problem, which enforces that the discretized level-set function (10) is equal to the initial level-set function at the Greville abscissas. The position of the Greville abscissas, shown in Figure 3, works as anchors for the B-splines and is computed as

$$\tilde{\xi}_i=\frac{\xi_{i+1}+\xi_{i+2}+...+\xi_{i+d}}{d}\qquad i=1,...,n. \tag{11}$$

During the optimization process, the evaluations of the level-set function at the Greville abscissas are updated, and the coefficients $c_{i,j}$ for the new level-set function discretization are obtained in the same process.

In Figure 4, we observe the identification process of the region where the element is located. This is achieved by evaluating the level-set function at a group of points in each element. Then, based on the sign of the evaluations, we can identify the region of the element and attribute the corresponding material property or, in the cut element, compute the average of it based on the cut ratio of the element, which is given as follows

$$\alpha|_T=\alpha_{out}+\frac{|T\cap\Omega|}{|T|}(\alpha_{in}-\alpha_{out}). \tag{12}$$

4 Topological Derivatives

In the previous sections, we defined the representation of a fixed domain D and a level-set function ϕ, used to represent the domain Ω, both by B-spline discretization. In the following, we discuss how the topological derivative is computed and how the level-set function is updated, focusing on minimizing the cost function.

Considering $\mathbf{x}_0\in D\setminus\partial\Omega$, and defining $\omega_\varepsilon(\mathbf{x}_o)=\{\mathbf{x}\in\mathbb{R}^2:||\mathbf{x}_0-\mathbf{x}||<\varepsilon\}$ as a circular perturbation with radius ε centered at $\mathbf{x}_0$. The introduction of the perturbation $\omega_\varepsilon(\mathbf{x}_o)$ in the domain D results in a perturbed domain

$$\Omega_\varepsilon=\begin{cases}\Omega\setminus\overline{\omega_\varepsilon(\mathbf{x}_0)} & \text{if } \mathbf{x}_0\in\Omega,\\ \Omega\cup\omega_\varepsilon(\mathbf{x}_0) & \text{if } \mathbf{x}_0\in D\setminus\overline{\Omega}.\end{cases} \tag{13}$$

Let $\mathcal{J}(\Omega):=J(\Omega,\mathbf{u}(\Omega))$ denote the reduced cost function where $\mathbf{u}(\Omega)$ denotes the unique solution to (1) for a given subdomain Ω. In this scenario, to measure the change in the cost function J when a new hole

around the point x_0 is introduced, the topological derivative is defined as

$$d\mathcal{J}(\Omega)(\mathbf{x}_0) := \lim_{\varepsilon \to 0} \frac{\mathcal{J}(\Omega_\varepsilon) - \mathcal{J}(\Omega)}{|\omega_\varepsilon|} = \lim_{\varepsilon \to 0} \frac{J(\Omega_\varepsilon, \mathbf{u}_\varepsilon) - J(\Omega, \mathbf{u})}{|\omega_\varepsilon|},$$

where $\mathbf{u}_\varepsilon$ is the solution of (1) replacing Ω by Ω_ε.

To evaluate this expression, we adopt the approach proposed in [18], which introduces the Lagrangian

$$L(\Omega, \mathbf{u}, \boldsymbol{\lambda}) = J(\Omega, \mathbf{u}) + \boldsymbol{\lambda} E(\Omega, \mathbf{u}),$$

where $E(\Omega, \mathbf{u}) = 0$ represents the weak form of the governing equation. This implies that $L(\Omega, \mathbf{u}, \boldsymbol{\lambda}) = J(\Omega, \mathbf{u})$ at the solution for all $\boldsymbol{\lambda}$. Consequently, the topological derivative can be rewritten as

$$d\mathcal{J}(\Omega)(\mathbf{x}_0) = \lim_{\varepsilon \to 0} \frac{L(\Omega_\varepsilon, \mathbf{u}_\varepsilon, \boldsymbol{\lambda}) - L(\Omega, \mathbf{u}, \boldsymbol{\lambda})}{|\omega_\varepsilon|}. \tag{14}$$

Plugging in the adjoint state $\boldsymbol{\lambda}$ defined as the solution of $\partial_{\mathbf{u}} L(\Omega, \mathbf{u}, \boldsymbol{\lambda}) = 0$, and noting that $\boldsymbol{\lambda} = -\frac{1}{2}\mathbf{u}$, after solving this limit for the linear elasticity problem, as shown in [6], an analytical expression is obtained, which depends only on the solution $\mathbf{u}$ and the material coefficient α

$$d\mathcal{J}(\Omega)(\mathbf{x}_0) = \begin{cases} d\mathcal{J}_{in}(\Omega)(\mathbf{x}_0) = -3\alpha_{in}\left(\dfrac{\alpha_{out} - \alpha_{in}}{2\alpha_{out} + \alpha_{in}}\right)\boldsymbol{\sigma}(\mathbf{u}) : \boldsymbol{\epsilon}(\mathbf{u}) - l & \text{if } \mathbf{x}_0 \in \Omega, \\ \\ d\mathcal{J}_{out}(\Omega)(\mathbf{x}_0) = -3\alpha_{out}\left(\dfrac{\alpha_{in} - \alpha_{out}}{2\alpha_{in} + \alpha_{out}}\right)\boldsymbol{\sigma}(\mathbf{u}) : \boldsymbol{\epsilon}(\mathbf{u}) + l & \text{if } \mathbf{x}_0 \in D \setminus \overline{\Omega}. \end{cases} \tag{15}$$

From this, the generalized topological derivative is then defined as

$$g_\Omega(\mathbf{x}) = \begin{cases} -d\mathcal{J}(\Omega)(\mathbf{x}) & \text{if } \mathbf{x} \in \Omega, \\ \\ d\mathcal{J}(\Omega)(\mathbf{x}) & \text{if } \mathbf{x} \in D \setminus \overline{\Omega}, \end{cases} \tag{16}$$

and used to update the level-set, guiding the evolution of the domain Ω. Algorithm 1 shows the update process. The update of the level-set is guided under a spherical linear interpolation, which uses the angle θ_i, in L^2-sense, between the current level-set ϕ_i and the topological derivative g_i, as a parameter to define the next domain Ω_{i+1}. Note that the stopping criterion is controlled by the same angle θ_i, and this quantity works as a comparison between the current topological derivative g_i and the level-set function ϕ_i. Then, if $\theta_i = 0$, the domain Ω_{i+1} is optimal and the topological derivative g_i can be used as the level-set function ϕ [7]. During this process, we apply a line search to define the parameter κ used to update the level-set

Algorithm 1: Level-set update

Initialize the level-set function ϕ_1;
for $i \leftarrow 1$ ***to*** n_{max} **do**
  Compute $g_{\Omega_i}(\mathbf{x}) = \begin{cases} -d\mathcal{J}(\Omega_i)(\mathbf{x}) & \text{if } \mathbf{x} \in \Omega_i, \\ d\mathcal{J}(\Omega_i)(\mathbf{x}) & \text{if } \mathbf{x} \in D \setminus \overline{\Omega_i}. \end{cases}$;
  Compute $\theta_i = \arccos\left(\frac{\langle \phi_i, g_{\Omega_i} \rangle}{||g_{\Omega_i}||_{L^2(D)} ||\phi_i||_{L^2(D)}}\right)$;
  if $\theta_i < \varepsilon_\theta$ **then**
    break;
  else
    $\phi_{i+1} = \frac{1}{\sin\theta_i}\left(\sin((1-\kappa_i)\theta_i)\phi_i + \sin(\kappa_i\theta_i) g_{\Omega_i}\right)$
    where $\kappa = \max\{1, \frac{1}{2}, \frac{1}{4}, \dots\}$ such that $\mathcal{J}(\Omega_{i+1}) < \mathcal{J}(\Omega_i)$;
  end
  Update c_{ij} in the discretization $\phi(\xi, \eta) = \sum_{i=1}^{n} \sum_{j=1}^{m} B_{i,d}(\xi) B_{j,d}(\eta) c_{ij}$
end
return ϕ;

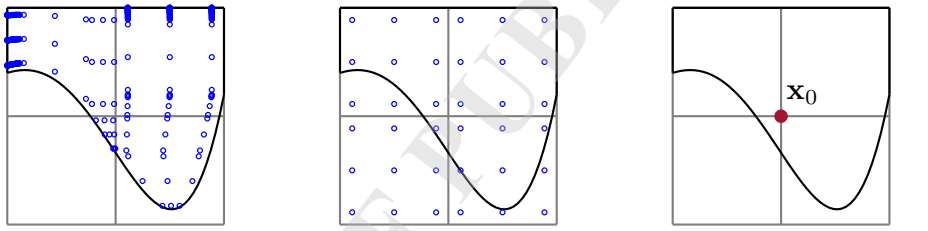

$|e \cap \Omega| = \sum_{j=1}^{nq^e} 1 \cdot w_j^e$ **a)** Cutratio computation

$K[e_i, e_j] = \alpha_e K_e[i, j]$ **b)** Integration for assembly

$g_\Omega(\mathbf{x}_0) = \frac{1}{n_e} \sum_{i=1}^{n_e} g_\Omega|_{e_i}(\mathbf{x}_0)$ **c)** Average filtering

Figure 5: Approaches to treat the cut elements

in the spherical linear interpolation. It is also applied some filtering processes, described in the section 5, to smooth the generalized topological derivative g, working similarly to a sensitivity filtering in density-based optimization [19]. In the discretized setting, when the element e of the background mesh D is cut by the interface of the level-set function ϕ, the generalized topological derivative is computed using a linear interpolation between the values computed inside and outside the domain Ω, given by

$$g_\Omega|_e(\mathbf{x}) = d\mathcal{J}_{out}(\Omega)(\mathbf{x})|_e + \frac{|e \cap \Omega|}{|e|}(-d\mathcal{J}_{in}(\Omega)(\mathbf{x})|_e - d\mathcal{J}_{out}(\Omega)(\mathbf{x})|_e). \tag{17}$$

5 Cut Elements

The correct integration of the elements intersected by the level-set function and the precision on defining the proper material parameter in these elements play an important role in the quality of the results. Therefore, in this section, we present the procedures used to deal with the cut elements.

In the computation of the cut ratio $|e \cap \Omega|/|e|$, necessary to obtain the α property for the cut elements, we apply a quadrature library for implicitly defined geometries [31, 32], which precisely follows the level-set function and provides quadrature points conforming with its zero isoline, as we can see in Figure 5a. This quadrature allows the integration of the regions defined by the zero level-set with high precision, also for complex geometries with high-degree representations of the interfaces. Therefore, with this quadrature, we can capture with precision the transition between the material property α in the inner part and the outer part of the domain Ω. Some examples for area computation, moving geometries, and linear elasticity can be seen in [39, 40].

However, when applying this precise quadrature rule for the assembly, we obtained some instabilities in the shape due to the integration of small parts of basis functions, located in the regions defined by the level-set function, and due to the jump between the material and the void regions, which results in a discontinuous field $\mathbf{u}$ and is approximated with higher-degree basis functions. To smooth these results, in the assembly process, we use the standard Gauss quadrature in the whole cut element and scale the local contribution by the corresponding material property α, computed using the previous procedure, shown in Figure 5b. Therefore, this approach smooths out the discontinuity in the transition between the elements and results in a shape with less noise.

Another smoothing step may be applied for the generalized topological derivative. In particular, since we define an α property at each element, it occurs that, when evaluating the derivative at a Greville point, shared by multiple elements, as we can see in Figure 5c, we have more than one α at the point. And to solve this, we consider the average of the derivative around that point. This procedure effectively creates a smooth transition where the material property changes and works well as a sensitivity filter [17].

A second filtering to smooth the generalized topological derivative g is performed by replacing g in the spherical linear interpolation, as described in Algorithm 1, by the solution $\tilde{g}$ of the PDE

$$\begin{aligned} -\gamma \Delta \tilde{g}_\Omega + \tilde{g}_\Omega &= g_\Omega \qquad \text{in } D \\ \nabla \tilde{g}_\Omega \cdot \mathbf{n} &= 0 \qquad \text{on } \partial D \end{aligned} \tag{18}$$

6 Numerical Results

In this section, two numerical results for different geometries are presented. In both examples, the level-set is initialized as $\phi(\mathbf{x}) = -1$, which results in a full material background mesh, and the background mesh is discretized with 128×128 elements. The material coefficients used are $\alpha_{in} = 1$ for the material region Ω and $\alpha_{out} = 10^{-4}$ for the void region $D \setminus \overline{\Omega}$. Additionally, the parameter for area control is $l = 5$, the

size control coefficient for the filtering is $\gamma = 10^{-4}$, and the Young modulus and the Poisson ratio are 1 and 1/3, respectively. In these examples, we investigate the sensitivity of the level-set function representation by applying different polynomial degrees d for the level-set function discretization and p for approximating the solution. This is done considering two settings. One with the level-set function and the solution, both approximated with the same polynomial degree, and another with a linear level-set function representation and a higher-degree approximation of the solution. For the optimization algorithm, we consider a tolerance of $\varepsilon_\theta = 1$ and a maximum number of iterations of 200.

6.1 Cantilever

The first example is the cantilever problem, a benchmark example for topology optimization present in a large number of research papers, see, e.g., [2, 3, 7, 35, 30, 22, 23, 24, 4]. In our case, the domain D is represented by the mapping from the parameter domain $\hat{D} = [0, 1] \times [0, 1]$ to a rectangle of size 2×1 with homogeneous Dirichlet boundary conditions on the left and a concentrated load on the right, as seen in Figure 6a. Figure 6b shows the final design for $p = d = 2$, and Figure 7 shows the evolution of the cost function, angle, and the area for the two settings. Additionally, the final shapes for different configurations of polynomial degree for the solution and the level-set function discretization are shown in Figure 8. A mesh sensitivity study with 32×32, 64×64, 128×128 and 256×256 elements is presented in Figure 9 and 10.

These results show that higher polynomial degrees p provide a better convergence behavior compared to $p = 1$, with a faster drop in the middle region of the graph in the Figure 7. However, since we use a fine mesh (128×128) to accurately represent the topology of the shape, increasing the polynomial degree p does not necessarily increase the accuracy of the solution. In addition, in all cases for this fine mesh, we converge to the same final solution (shown in Figure 8), with similar convergence paths for higher degrees p, and the same number of steps is required for $p = 2$ and $p = 4$ in both level-set discretization settings, see Figure 7. However, when using $p = 3$, 29 steps are required for the higher-degree level-set discretization ($d = p$),

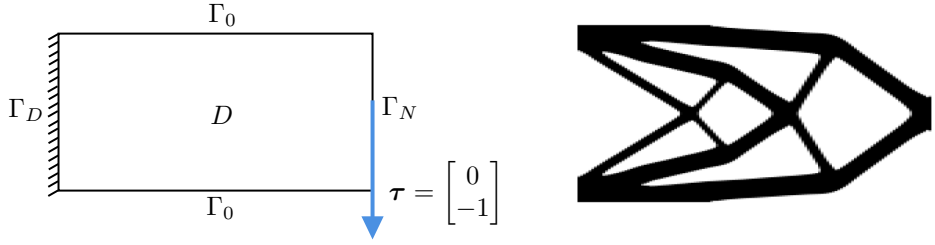

a) Initial problem **b)** Final shape

Figure 6: Cantilever problem

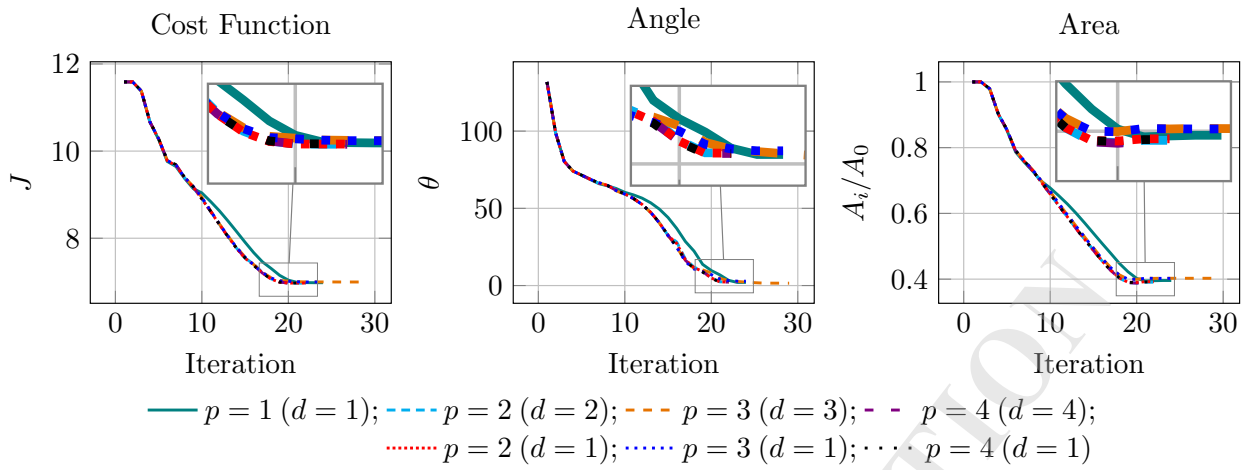

Figure 7: Comparison of the evolution of the cost function, angle, and area for different polynomial degrees of solution approximation, with a linear level-set function representation (dotted), and with a level-set function representation with the same polynomial degree as the solution approximation (dashed).

compared to 24 for the linear level-set discretization ($d = 1$). We also observe a slight difference in the final part of the area graph between different solution discretizations using odd and even B-spline degrees. This difference happens because in the Greville abscissae for odd degrees, some points are shared between elements. As a result, an averaging is performed around these positions when evaluating the solution, effectively acting as a filtering process [17]. While this helps to smooth the solution, it introduces a small difference compared to cases where such averaging is not required.

Figure 9 and 10 show the impact of the background mesh resolution on the final shape. As our optimization problem is not convex, it is reasonable to expect different topologies for different mesh sizes (e.g., Figure 10a for $p = d = 1$, and Figure 10b for $p = d = 3$). For $p = d = 2$, however, similar final topologies are obtained for all different mesh sizes. In addition, since we can represent the design more accurately with decreasing mesh size (i.e., the design space is growing), we are able to find better local minima with decreasing function values from 8.58 (Figure 10a, $p = d = 2$) to 6.97 (Figure 10c, $p = d = 2$). Comparing the results using our standard mesh (128×128, Figure10c) to the finest one (256×256, Figure10d), we observe the same designs with minor variations in the objective value for all polynomial degrees. In Figure 9, the evolutions of the cost functional for $p = d = 2$ and $p = d = 3$ in the meshes 128×128 and 256×256 are identical. This demonstrates that our method is mesh-independent, i.e., stable with respect to further mesh refinements, with the minimal feature size related to the filtering of the topological derivative (18).

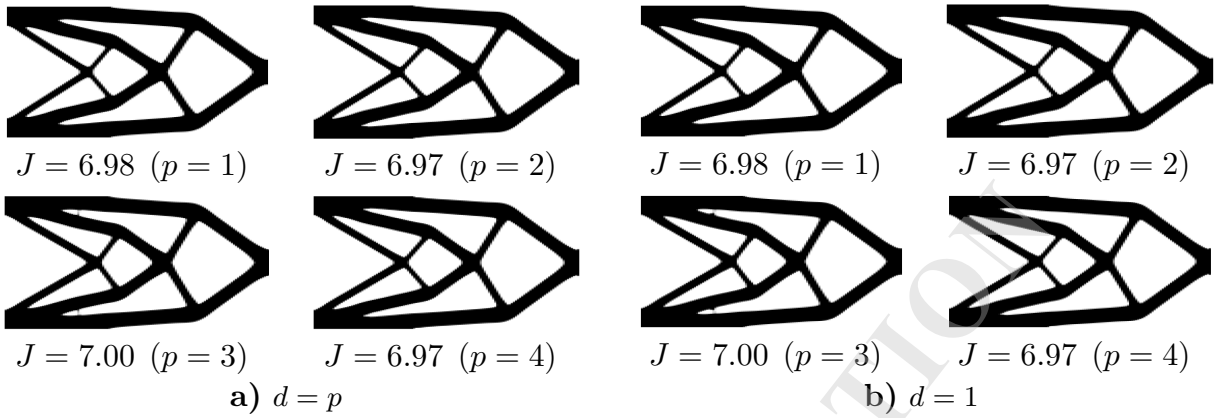

Figure 8: Final shape for different basis functions degree for approximating the solution: a) Level-set discretized with the same polynomial degree as the solution. b) Level-set discretized with linear basis functions

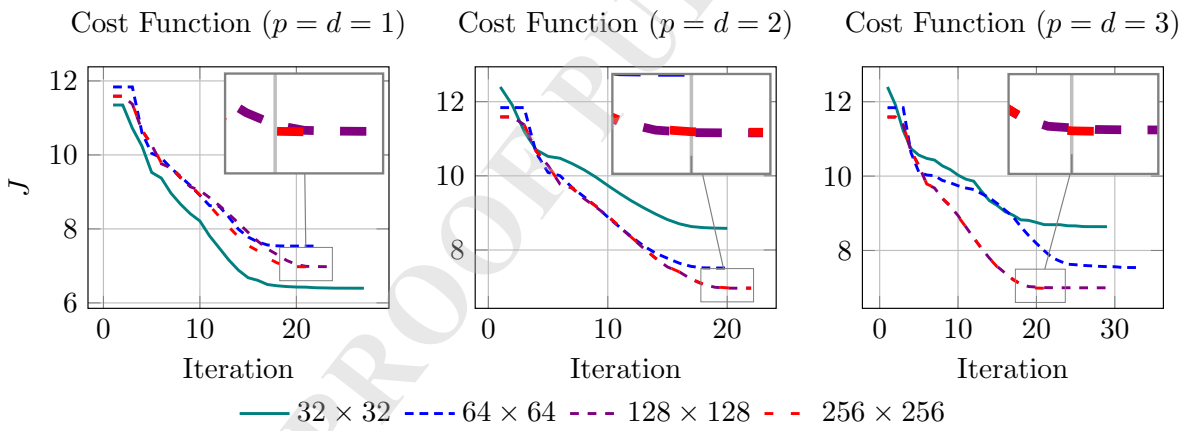

Figure 9: Comparison of the evolution of the cost function for different mesh resolutions, using the same polynomial degrees for solution approximation and level-set function representation.

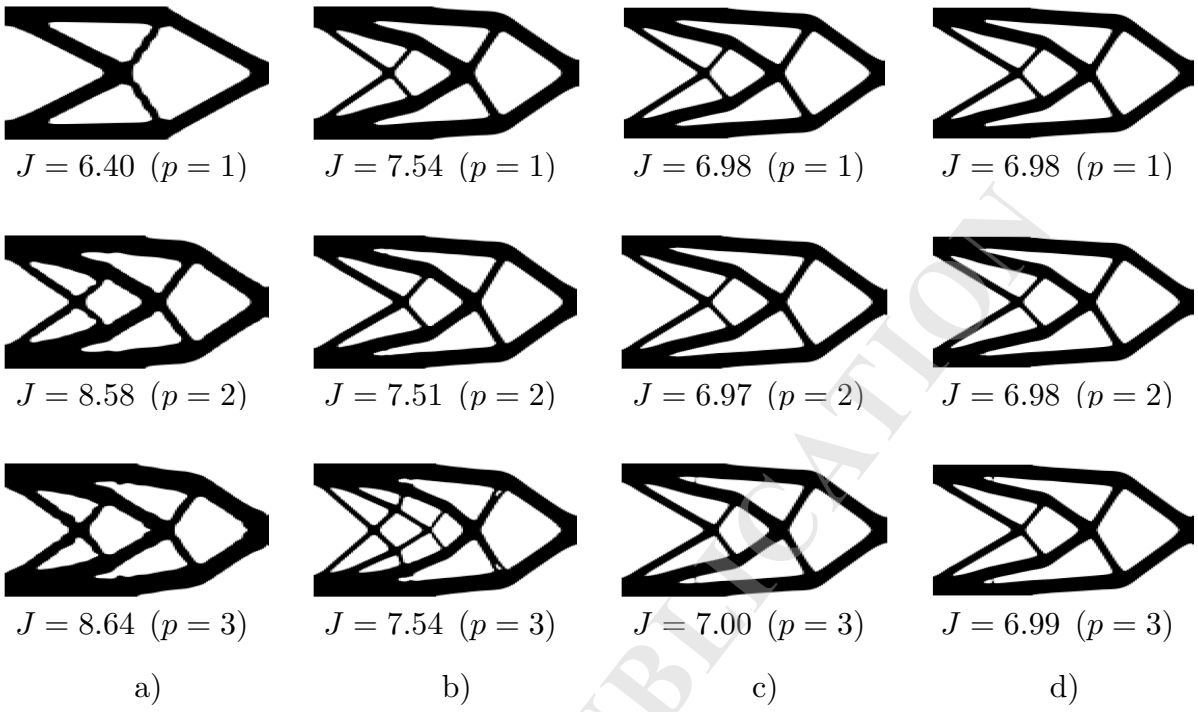

Figure 10: Final shape for $p = d$ and meshes using different numbers of elements per direction: a) 32×32, b) 64×64, c) 128×128, d) 256×256

6.2 Quarter Ring

This example is also considered in several research papers [14, 22, 4, 5], where the same geometry is applied under different approaches and loading configurations. In our example, the domain D is defined by a mapping from the parameter domain $\hat{D} = [0, 1] \times [0, 1]$ to a quarter of a ring with inner radius $R_{in} = 1$ and outer radius $R_{out} = 2$. Homogeneous Dirichlet boundary conditions are imposed on the bottom boundary, and a concentrated load is applied at $(0, 2)$, as illustrated in Figure 11a. The final design for $p = d = 3$

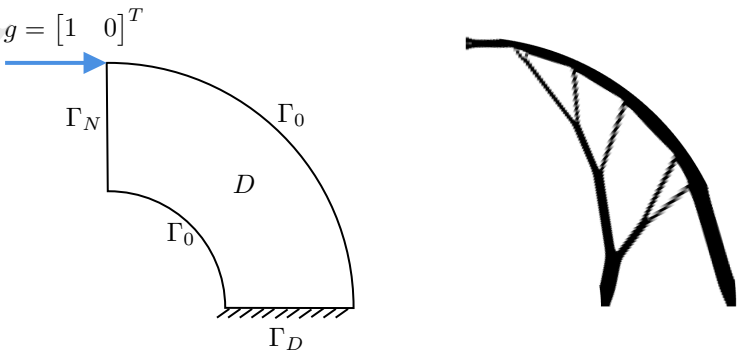

a) Initial problem **b)** Final shape

Figure 11: Curved cantilever problem

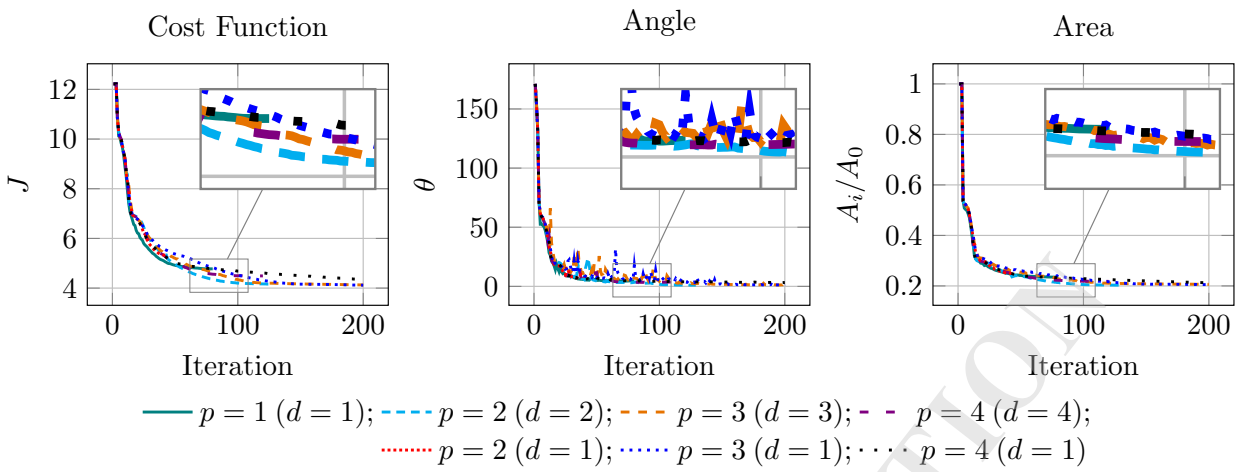

Figure 12: Comparison of the evolution of the cost function, angle, and area for different polynomial degrees of solution approximation, with a linear level-set function representation (dotted), and with a level-set function representation with the same polynomial degree as the solution approximation (dashed).

is shown in Figure 11b, while the evolution of the level-set function and the corresponding final shapes are presented in Figure 12 and 13, respectively.

From these results, we observe that for $p = 1(d = 1)$ and $p = 2(d = 1)$ the optimization stops for 80 and 43 iterations, with angles θ equal to 4.72 and 9.33, respectively, while in all of the remaining simulations an angle $\theta < 4$ is reached, which is a reasonable value for a numerical solutions [7]. We also notice that, although the cost function converges to a similar minimum value, all the shapes present different solutions with different configurations of features. Regarding the minimization, the lowest cost function values are obtained for $p = 3(d = 1)$ with 4.12 and $p = 3(d = 3)$ with 4.13, both with 200 iterations. While, for $p = 2(d = 2)$, a slightly higher value of 4.15 is obtained, but requires only 129 iterations.

In topology optimization, the presence of a local minimum is a well-known challenge and has a dependence on the choice of initial parameters [37]. Small variations in the definition of the initial setting of parameters can lead to different solutions. As a result, even if the initialization is too far from the global minimum, we still can achieve a solution that converges to a local minimum [3]. Therefore, while strategies like refining the mesh in a coarse-to-fine approach can partially cure this issue, they do not eliminate it [1]. In this example, we notice that the possibility of setting different configurations of polynomial degrees, for the level-set discretization and the solution approximation, does not overcome this phenomenon completely, but depending on the choice of setting, we can obtain a solution that satisfies the condition of having a small θ. Another parameter that can be changed and opens the possibility to find different solutions is the parameter γ, which limits the size of features in the filtering process, overcoming some noise in the final shape.

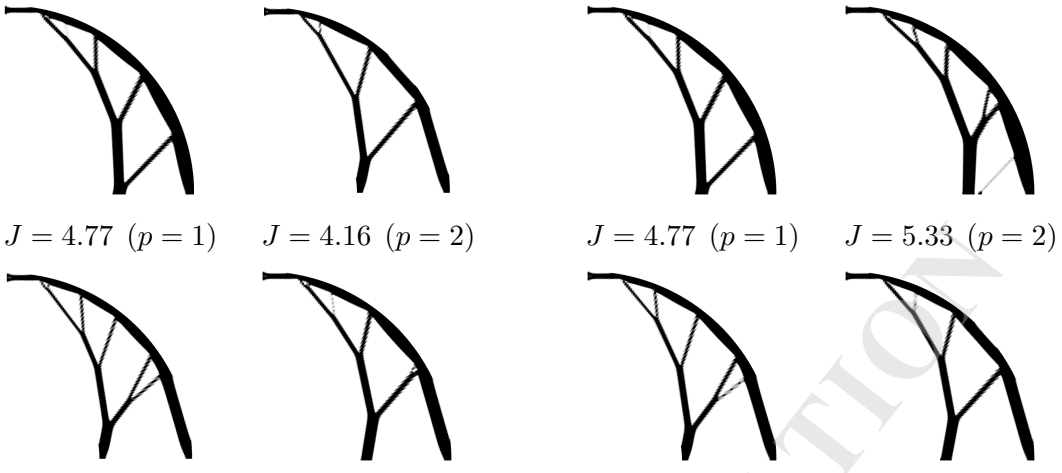

Figure 13: Final shape for different basis functions degree for approximating the solution: a) Level-set discretized with the same polynomial degree as the solution. b) Level-set discretized with linear basis functions.

7 Conclusion

In this work, we develop an immersed isogeometric approach for a level-set based topology optimization guided only by the topological derivative. The isogeometric approach within this framework provides a seamless geometry update due to a simplified mesh process, defined by a knot vector and control points. It also facilitates straightforward higher-order simulations, yielding results that are comparable to or slightly better than those obtained by the standard approach. In addition, we also treat the elements cut by the level-set function using a quadrature library for implicitly defined geometries to compute a material property used to neglect the contributions from outside the domain Ω, and using a filtering process to smooth the change of material between elements.

This study investigates the impact of using higher-degree basis functions in both the approximation of the solution and the discretization of the level-set function. In this investigation, we observe that being able to perform higher-order simulations can be beneficial, in terms of iterations or the final cost function. However, regarding the level-set discretization, we observe that using linear basis functions yields results comparable to those obtained with higher-degree polynomials. Therefore, although the level-set is continuous, there is a discontinuity in the material property between the material region and the void. Our results indicate that using higher-degree basis functions does not directly imply a better representation of the jump across the interface. We will further investigate this aspect in future research. In addition, the proposed approach is currently limited to a single-patch background geometry, and the extension for multi-patch structures is also

a subject for future research.

8 Acknowledgement

This work is supported by the joint DFG/FWF Collaborative Research Centre CREATOR (CRC – TRR361/F90; Grant-DOI 10.55776/F90) at TU Darmstadt, TU Graz, RICAM and JKU Linz. Moreover, P. G. is partially supported by the State of Upper Austria.

References

[1] G. Allaire and F. Jouve. Coupling the level set method and the topological gradient in structural optimization, [in:] *Proceedings IUTAM Symposium on Topological Design Optimization of Structures, Machines and Materials*, pp. 3-12. Dordrecht, 2006. doi: https://doi.org/10.1007/1-4020-4752-5_1.

[2] G. Allaire, F. Jouve, and A. Toader. A level-set method for shape optimization. *C. R. Acad. Sci. Paris, Ser. I*, **334**:1125–1130, 2002. doi: https://doi.org/10.1016/S1631-073X(02)02412-3.

[3] G. Allaire, F. Jouve, and A. Toader. Structural optimization using sensitivity analysis and a level-set method. *Journal of Computational Physics*, **194**:363–393, 2 2004. doi: https://doi.org/10.1016/j.jcp.2003.09.032.

[4] M. Aminzadeh and S. M. Tavakkoli. A parameter space approach for isogeometrical level set topology optimization. *International Journal for Numerical Methods in Engineering*, **123**:3485–3506, 8 2022. doi: https://doi.org/10.1002/nme.6976.

[5] M. Aminzadeh and S. M. Tavakkoli. Multiscale topology optimization of structures by using isogeometrical level set approach. *Finite Elements in Analysis and Design*, **235**, 8 2024. doi: https://doi.org/10.1016/j.finel.2024.104167.

[6] S. Amstutz. Sensitivity analysis with respect to a local perturbation of the material property. *Asymptotic Analysis*, **49**(1-2):87–108, 2006. doi: https://doi.org/10.3233/ASY-2006-778.

[7] S. Amstutz and H. Andrä. A new algorithm for topology optimization using a level-set method. *Journal of Computational Physics*, **216**:573–588, 8 2006. doi: https://doi.org/10.1016/j.jcp.2005.12.015.

[8] S. Amstutz, A. A. Novotny, and E. A. De Souza Neto. Topological derivative-based topology optimization of structures subject to drucker-prager stress constraints. *Computer Methods in Applied Mechanics and Engineering*, **233-236**:123–136, 8 2012. doi: https://doi.org/10.1016/j.cma.2012.04.004.

[9] M. P. Bendsøe and N. Kikuchi. Generating optimal topologies in structural design using a homogenization method. *Computer Methods in Applied Mechanics and Engineering*, **71**:197–224, 1988. doi: https://doi.org/10.1016/0045-7825(88)90086-2.

[10] M. Burger, B. Hackl, and W. Ring. Incorporating topological derivatives into level set methods. *Journal of Computational Physics*, **194**:344–362, 2 2004. doi: https://doi.org/10.1016/j.jcp.2003.09.033.

[11] F. S. Carvalho, D. Ruscheinsky, S. M. Giusti, C. T.M. Anflor, and A. A. Novotny. Topological derivative-based topology optimization of plate structures under bending effects. *Structural and Multidisciplinary Optimization*, **63**:617–630, 2 2021. doi: https://doi.org/10.1007/s00158-020-02710-4.

[12] F. de Prenter, C. V. Verhoosel, E. H. van Brummelen, M. G. Larson, and S. Badia. Stability and conditioning of immersed finite element methods: Analysis and remedies. *Archives of Computational Methods in Engineering*, **30**:3617–3656, 7 2023. doi: https://doi.org/10.1007/s11831-023-09913-0.

[13] J. D. Deaton and R. V. Grandhi. A survey of structural and multidisciplinary continuum topology optimization: Post 2000. *Structural and Multidisciplinary Optimization*, **49**:1–38, 1 2014. doi: https://doi.org/10.1007/s00158-013-0956-z.

[14] L. Dedè, M. J. Borden, and T. J.R. Hughes. Isogeometric analysis for topology optimization with a phase field model. *Archives of Computational Methods in Engineering*, **19**:427–465, 9 2012. doi: https://doi.org/10.1007/s11831-012-9075-z.

[15] F. Feppon, G. Allaire, C. Dapogny, and P. Jolivet. Body-fitted topology optimization of 2d and 3d fluid-to-fluid heat exchangers. *Computer Methods in Applied Mechanics and Engineering*, 376:113638, 2021. ISSN 0045-7825. doi: https://doi.org/10.1016/j.cma.2020.113638. URL `https://www.sciencedirect.com/science/article/pii/S0045782520308239`.

[16] J. M. M. Luz Filho, R. Mattoso, and L. Fernandez. A freefem code for topological derivative-based structural optimization. *Structural and Multidisciplinary Optimization*, **66**, 4 2023. doi: https://doi.org/10.1007/s00158-023-03529-5.

[17] P. Gangl. A multi-material topology optimization algorithm based on the topological derivative. *Computer Methods in Applied Mechanics and Engineering*, **366**, 7 2020. doi: https://doi.org/10.1016/j.cma.2020.113090.

[18] P. Gangl and K. Sturm. A simplified derivation technique of topological derivatives for quasi-linear

transmission problems. *ESAIM - Control, Optimisation and Calculus of Variations*, **26**, 2020. doi: https://doi.org/10.1051/cocv/2020035.

[19] P. Gangl, T. Komann, N. Krenn, and S. Ulbrich. Robust topology optimization of electric machines using topological derivatives. *Arxiv*, 4 2025. URL `http://arxiv.org/abs/2504.05070`.

[20] J. Gao, M. Xiao, Y. Zhang, and L. Gao. A comprehensive review of isogeometric topology optimization: Methods, applications and prospects. *Chinese Journal of Mechanical Engineering (English Edition)*, **33**:14, 12 2020. doi: https://doi.org/10.1186/s10033-020-00503-w.

[21] T.J.R. Hughes, J. A. Cottrell, and Y. Bazilevs. Isogeometric analysis: Cad, finite elements, nurbs, exact geometry and mesh refinement. *Computer Methods in Applied Mechanics and Engineering*, **194**:4135–4195, 10 2005. doi: https://doi.org/10.1016/j.cma.2004.10.008.

[22] H. A. Jahangiry and S. M. Tavakkoli. An isogeometrical approach to structural level set topology optimization. *Computer Methods in Applied Mechanics and Engineering*, **319**:240–257, 6 2017. doi: https://doi.org/10.1016/j.cma.2017.02.005.

[23] M. Khatibinia, M. Khatibinia, and M. Roodsarabi. Structural topology optimization based on hybrid of piecewise constant level set method and isogeometric analysis. *International Journal of Optimization in Civil Engineering*, **10**:493–512, 2020. URL `https://www.researchgate.net/publication/342924423`.

[24] N. Krenn. Multi-material topology optimization subject to pointwise stress constraints for Additive Manufacturing. Master's thesis, Graz University of Technology, 2021.

[25] C. G. Lopes, R. B. dos Santos, and A. A. Novotny. Topological derivative-based topology optimization of structures subject to multiple load-cases. *Latin American Journal of Solids and Structures*, **12**:834–860, 9 2015. doi: https://doi.org/10.1590/1679-78251252.

[26] B. Ma, J. Zheng, G. Lei, J. Zhu, P. Jin, and Y. Guo. Topology optimization of ferromagnetic components in electrical machines. *IEEE Transactions on Energy Conversion*, **35**:786–798, 6 2020. doi: https://doi.org/10.1109/TEC.2019.2960519.

[27] E. A. De Souza Neto, S. Amstutz, S. M. Giusti, and A. A. Novotny. Topological derivative-based optimization of micro-structures considering different multi-scale models. *Computer Modeling in Engineering & Sciences*, **62**:23–54, 2010. doi: https://doi.org/10.3970/cmes.2010.062.023.

[28] A. A. Novotny, C. G. Lopes, and R. B. Santos. Topological derivative-based topology optimization of structures subject to self-weight loading. *Structural and Multidisciplinary Optimization*, **63**:1853–1861, 4 2021. doi: https://doi.org/10.1007/s00158-020-02780-4.

[29] S. Osher and J. A. Sethian. Fronts propagating with curvature-dependent speed: Algorithms based on hamilton-jacobi formulations. *Journal of Computational Physics*, **79**:12–49, 1988. doi: https://doi.org/10.1016/0021-9991(88)90002-2.

[30] M. Roodsarabi, M. Khatibinia, and S. R. Sarafrazi. Hybrid of topological derivative-based level set method and isogeometric analysis for structural topology optimization. *Steel and Composite Structures*, **21**:1389–1410, 8 2016. doi: https://doi.org/10.12989/scs.2016.21.6.1389.

[31] R. I. Saye. High-order quadrature methods for implicitly defined surfaces and volumes in hyperrectangles. *SIAM Journal on Scientific Computing*, **37**:A993–A1019, 2015. doi: https://doi.org/10.1137/140966290.

[32] R. I. Saye. High-order quadrature on multi-component domains implicitly defined by multivariate polynomials. *Journal of Computational Physics*, **448**, 1 2022. doi: 10.1016/j.jcp.2021.110720.

[33] D. Schillinger and M. Ruess. The finite cell method: A review in the context of higher-order structural analysis of cad and image-based geometric models. *Archives of Computational Methods in Engineering*, **22**:391–455, 7 2015. doi: https://doi.org/10.1007/s11831-014-9115-y.

[34] E. Shakour and O. Amir. Topology optimization with precise evolving boundaries based on iga and untrimming techniques. *Computer Methods in Applied Mechanics and Engineering*, **374**, 2 2021. doi: https://doi.org/10.1016/j.cma.2020.113564.

[35] S. Shojaee, M. Mohamadian, and N. Valizadeh. Composition of isogeometric analysis with level set method for structural topology optimization. *International Journal of Optimization in Civil Engineering*, **2**:47–70, 2012. URL `https://www.researchgate.net/publication/259593893`.

[36] O. Sigmund and K. Maute. Topology optimization approaches: A comparative review. *Structural and Multidisciplinary Optimization*, **48**:1031–1055, 12 2013. doi: https://doi.org/10.1007/s00158-013-0978-6.

[37] O. Sigmund and J. Petersson. Numerical instabilities in topology optimization: A survey on procedures dealing with checkerboards, mesh-dependencies and local minima. *Structural Optimization*, **16**:68–75, 1998. doi: https://doi.org/10.1007/BF01214002.

[38] P. Suttakul, H. T. Ngo, M. N. Nguyen, T. Q. Bui, J. Rungamornrat, and D. Vo. Isogeometric proportional topology optimization (iga-pto) for multi-material problems. *Mechanics of Advanced Materials and Structures*, **32**:5006–5025, 2025. doi: https://doi.org/10.1080/15376494.2024.2418352.

[39] G. H. Teixeira, M. Loibl, and B. Marussig. Comparison of integration methods for cut elements. *ArXiv*, 1 2025. doi: https://doi.org/10.23967/eccomas.2024.098. URL `http://arxiv.org/abs/2501.03854`.

[40] T. Toprak, M. Loibl, G. H. Teixeira, I. Shishkina, C. Miao, J. Kiendl, B.Marussig, and F. Kummer. Employing continuous integration inspired workflows for benchmarking of scientific software — a use case on numerical cut element quadrature. *Advances in Engineering Software*, **213**:104087, 2026. doi: https://doi.org/10.1016/j.advengsoft.2025.104087.

[41] R. Verzicco. Immersed boundary methods: Historical perspective and future outlook. *Annual Review of Fluid Mechanics*, **11**:39, 2023. doi: https://doi.org/10.1146/annurev-fluid-120720.

[42] D. Vo, M. N. Nguyen, T. Q. Bui, P. Suttakul, and J. Rungamornrat. Isogeometric gradient-free proportional topology optimization (iga-pto) for compliance problem. *International Journal for Numerical Methods in Engineering*, **124**:4275–4310, 10 2023. doi: https://doi.org/10.1002/nme.7315.

[43] R. Vázquez. A new design for the implementation of isogeometric analysis in octave and matlab: Geopdes 3.0. *Computers and Mathematics with Applications*, **72**:523–554, 8 2016. doi: https://doi.org/10.1016/j.camwa.2016.05.010.

[44] M. Y. Wang, X. Wang, and D. Guo. A level set method for structural topology optimization. *Computer Methods in Applied Mechanics and Engineering*, **192**:227–246, 2003. doi: https://doi.org/10.1016/S0045-7825(02)00559-5.

[45] X. S. Wang, L. T. Zhang, and W. K. Liu. On computational issues of immersed finite element methods. *Journal of Computational Physics*, **228**:2535–2551, 4 2009. doi: https://doi.org/10.1016/j.jcp.2008.12.012.

[46] M. Wiesheu, T. Komann, M. Merkel, S. Schöps, S. Ulbrich, and I. Cortes Garcia. Combined parameter and shape optimization of electric machines with isogeometric analysis. *Optimization and Engineering*, **26**:1011–1038, 2024. doi: https://doi.org/10.1007/s11081-024-09925-0.

[47] M. Xavier and A. A. Novotny. Topological derivative-based topology optimization of structures subject

to design-dependent hydrostatic pressure loading. *Structural and Multidisciplinary Optimization*, **56**: 47–57, 7 2017. doi: https://doi.org/10.1007/s00158-016-1646-4.